Effect of rotation on heat transfer in two-pass square channels with five different orientations of 45° angled rib turbulators

Luai Al-Hadhrami, Je-Chin Han [*]

Turbine Heat Transfer Laboratory, Department of Mechanical Engineering, Texas A&M University, College Station, TX 77843-3123, USA

Received 17 October 2001; received in revised form 3 August 2002

Abstract

The effect of various 45° angled rib turbulator arrangements on the Nusselt number ratio in a rotating, two-pass, square channel is investigated for three Reynolds numbers (5000, 10,000, 25,000), with rotation number up to 0.11, and two channel orientations with respect to the axis of rotation ($\beta = 90°$ and 135°). Five different arrangements of rib turbulators are placed on the leading and trailing surfaces at an angle of $+45°$ or $-45°$ to the main stream flow. The rib height-to-hydraulic diameter ratio (e/D) is 0.125; the rib pitch-to-height ratio (P/e) is 10; and the inlet coolant-to-wall density ratio ($\Delta\rho/\rho$) is maintained around 0.11. The results show that the rotating ribbed surface Nusselt number ratios increase by a factor of 2 compared to the rotating smooth surface results. The results also show that the heat transfer enhancement depends on the rib-angle orientation ($+45°$ or $-45°$) to the main stream flow in the first or second pass of the channel for both rotating and non-rotating conditions. Overall, the parallel rib cases show better heat transfer enhancement than the crossed rib case for both rotating and non-rotating conditions. The 90° channel orientation with respect to the axis of rotation produces greater rotating effect on heat transfer over the 135° channel orientation.
© 2002 Elsevier Science Ltd. All rights reserved.

1. Introduction

As gas turbine technology continues to advance (driven by increasing thermal efficiency and power output), a more sophisticated cooling system designs is necessary. In advanced gas turbines, turbine blades encounter high thermal loads caused by temperatures which can exceed the melting point of the metal to achieve maximum efficiency. Internal airfoil cooling technology is used to maintain acceptable metal temperatures. Internal cooling typically consists of complex cooling passage channel configurations embedded within the turbine blade airfoil. These channels are connected by 180° turns and roughened by angled rib turbulators to enhance cooling effect. When the turbine blade experiences rotation, Coriolis and buoyancy forces induce secondary flows that interact with the rib-induced secondary flows to further complicate the flow. Therefore, both the nature of the flow and the associated convection heat transfer are usually significantly altered through the rotating ribbed channels and the 180° turns. The average heat transfer enhancement is usually desirable, but the variation in heat transfer around the channel cross-section and within the 180° turn is often not desirable. Therefore, such variations in heat transfer rate occurring over small distances can lead to increased thermal stresses and decrease the blade life. It is of the primary interest to find combined parameters (such as angle rib orientation and rib angle of attack to the main flow stream) which enhance heat transfer and do not lead to the creation of large thermal stress zones within the blade.

Earlier studies on cooling passages were primarily based on stationary models. However, stationary models neglect the Coriolis and buoyancy effects which alter the

[*] Corresponding author. Tel.: +1-979-845-3738; fax: +1-979-862-2418/+1-979-862-2418.

E-mail address: jchan@mengr.tamu.edu (J.-C. Han).

Nomenclature

D	hydraulic diameter (m)	Ro	rotation number $\Omega D/V$
E	rib height (m)	V	average axial flow velocity (m/s)
h	heat transfer coefficient (W/m^2 °C)	μ	viscosity of air (kg/m s)
K	thermal conductivity of coolant (W/m K)	Ω	rotational speed (rad/s)
L	length of the duct (m)	ρ	density of air (kg/m^3)
Nu	Nusselt number, hD/K	T_{bx}	local bulk mean coolant temperature (°C)
Nu_o	Nusselt number in fully developed smooth-walled turbulent pipe flow	T_w	local wall temperature (°C)
		T_{bi}	inlet coolant temperature (°C)
P	rib pitch (m)	$\Delta\rho/\rho$	inlet coolant-to-wall density ratio $(T_w - T_{bi})/T_w$
q_{net}	net heat at wall (W)		
A	surface area of the copper plate (m^2)	β	angle of the channel orientation with respect
Re	Reynolds number $\rho VD/\mu$		to the axis of rotation

velocity, turbulence and temperature distributions. Metzger and Sahm [1] studied forced convection in a smooth rectangular channel by varying the divider location and the gap at the 180° turn. Fan and Metzger [2] extended the work by Metzger by varying the channel width. They concluded that increasing the channel aspect ratio results in smaller azimuthal heat transfer variations and increased overall channel heat transfer. Han et al. [3] studied the local heat/mass transfer distribution in a non-rotating two-pass ribbed channel. Han and Zhang [4] studied the effect of rib-angle orientation on local heat/mass transfer distribution in a non-rotating three-pass rib-roughened channel. It was observed that the rib angle, rib orientation, and the sharp 180° turn significantly affected the local heat/mass transfer distributions. The combined effects of these parameters increased and decreased the local heat/mass transfer coefficients after the sharp 180° turns. Han et al. [5] studied the effect of the rib-angle orientation on heat transfer distributions and pressure drop in a non-rotating square channel with opposite, in-line ribbed walls. They found that the 60° and 45° V-shaped ribs performed better than the 60° and 45° crossed ribs and 90° transverse ribs. Ekkad and Han [6] performed a detailed study on heat transfer characteristics in a non-rotating square channel with a sharp 180° turn using a transient liquid crystal technique. One wall of the channel had periodically placed rib turbulators. Four different configurations of 90° parallel, 60° parallel, 60° V-shaped, and 60° inverted V-shaped ribs were discussed. Ekkad et al. [7] repeated the same experiment, but with bleed holes placed between the ribs. They confirmed that the 60° V-shaped ribs performed better than the 60° parallel and 60° inverted V-shaped ribs.

More recently, experiments with rotation have been conducted to more closely model engine cooling environments. Wagner et al. [8,9] conducted a detailed experimental study to determine the effects of rotation

(buoyancy and Coriolis forces) on the local heat transfer of a multi-pass square channel with smooth walls. They concluded that the first pass of the coolant passage with rotation created a thinner boundary layer on the trailing surface and a thicker boundary layer on the leading surface resulting in increased heat transfer and decreased heat transfer, respectively. In the second pass the performance was different and opposite that of the first pass. The leading surface Nusselt number ratios in the second pass were higher than the trailing surface Nusselt number ratios because of the reversal of the Coriolis force direction. Taslim et al. [10,11] investigated the heat transfer distribution in square and rectangular rib-roughened channels under rotation. They found that the effects of rotation were more apparent in rib-roughened channels with a larger channel aspect ratio and a lower rib blockage ratio. Johnson et al. [12] performed a parametric experiment to investigate the effects of buoyancy and Coriolis forces on the heat transfer coefficient distribution of four-pass square channels with 45° angled ribs. Johnson et al. [13] conducted experimental work to determine the effects of channel orientation with respect to axis of rotation as well as buoyancy and Coriolis forces on heat transfer in turbine blade internal coolant passages. The experiments were conducted with rotation in both directions to simulate serpentine coolant passages with the rearward flow of coolant or with the forward flow of coolant. They concluded that both the rotation and channel orientation could change the leading and trailing surface heat transfer coefficients of the ribbed channel. Han et al. [14] investigated the uneven wall temperature effect on local heat transfer in a rotating two-pass square channel with smooth walls. They concluded that uneven surface temperatures on the leading and trailing surfaces create unequal local buoyancy forces, which alter heat transfer coefficients. Zhang et al. [15] analyzed the heating condition effects in a duct with angled rib turbulators with

rotation. They found that an uneven wall temperature had a significant impact on the local heat transfer co-efficients. Parsons et al. [16,17] studied the effects of channel orientation and wall heating condition on the local heat transfer coefficient in a rotating two-pass square channel with ribbed walls. They found that the effects of the Coriolis force and cross-stream flow were reduced as the channel orientation changed from the normal $\beta = 90°$ to an angled orientation of $\beta = 135°$. Dutta and Han [18] also investigated the local heat transfer coefficients in rotating smooth and ribbed, two-pass square channels with three channel orientations. Dutta et al. [19] presented experimental heat transfer results for turbulent flow through a rotating two-pass rib-roughened triangular channel for two channel orientations with respect to the axis of rotation. In addi-tion, Park and Lau [20] and Park et al. [21] conducted experimental work using Naphthalene sublimation to study the effects of the Coriolis force, 180° turn, channel orientation, and the different rib arrangements on local heat/mass transfer distributions on the leading and trailing walls of a two-pass square channel. For a more comprehensive compilation of turbine heat transfer re-search, please see the book by Han et al. [22].

It is clear that from the above-mentioned research, the existence of the angled ribs (placed at an angle to the main coolant flow direction) enhances the heat transfer coefficient due to increased turbulence mixing, second-ary flow, and, to some extent, due to increased surface area. Meanwhile, it has been shown in the literature that parallel ribs perform better than the crossed ribs under non-rotating conditions. However, it is interesting to

1. Electircal Motor with Controller   **6. Rotating Arm**
2. Rotating Shaft   **7. Test Section**
3. Belt Drive Pulley System   **8. Compressor Air**
4. Bearing Support System   **9. Rotory Seal**
5. Steel Table   **10. Slip Ring**
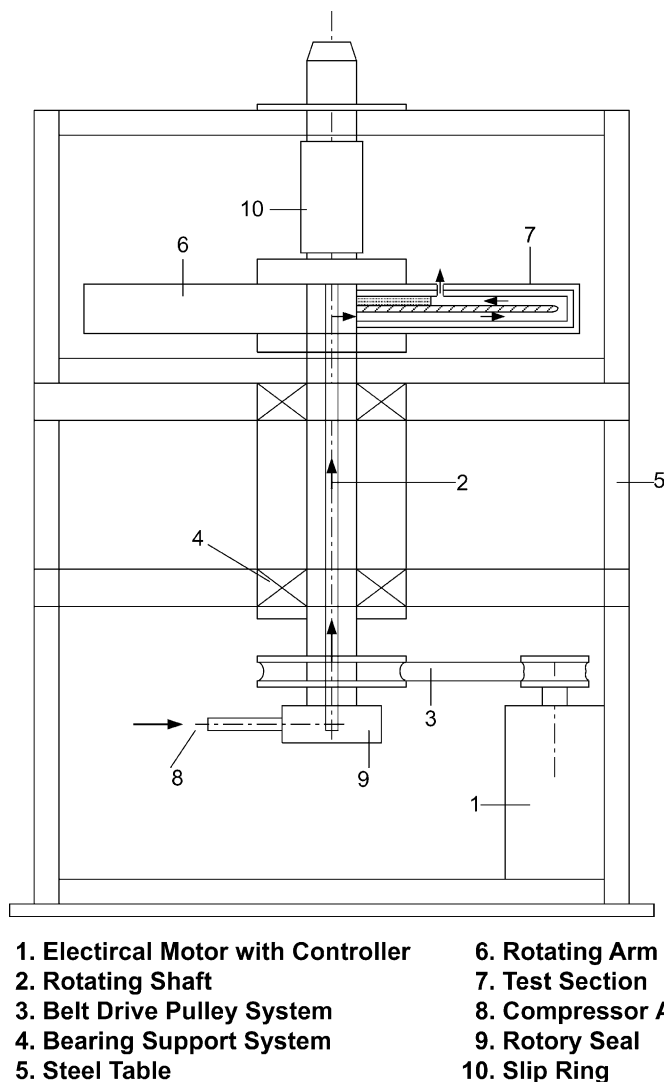
Fig. 1. Schematic view for the test rig.

know whether this holds true under rotating conditions. In addition, as the secondary flows resulting from rotational effects interact with rib-induced secondary flows and the sharp 180° flow turns, new characteristics in heat transfer with rotation are expected. Therefore, the objectives of this paper are to study:

1. The effects of the parallel rib-angle orientation on the heat transfer distribution in a rotating two-pass square channel.
2. The effects of the parallel rib-angle orientation in the sharp 180° turn on the heat transfer distribution.

3. The performance of the crossed rib-angle orientation (the angled ribs on two opposite surfaces of the cooling channels are in crossed orientations), and to compare it to the parallel rib cases.
4. The effects of the channel orientation with respect to the axis of rotation.

2. Description of the experiment

Fig. 1 shows the schematic of the test rig. Compressed air, regulated across a sharp-edge orifice flow
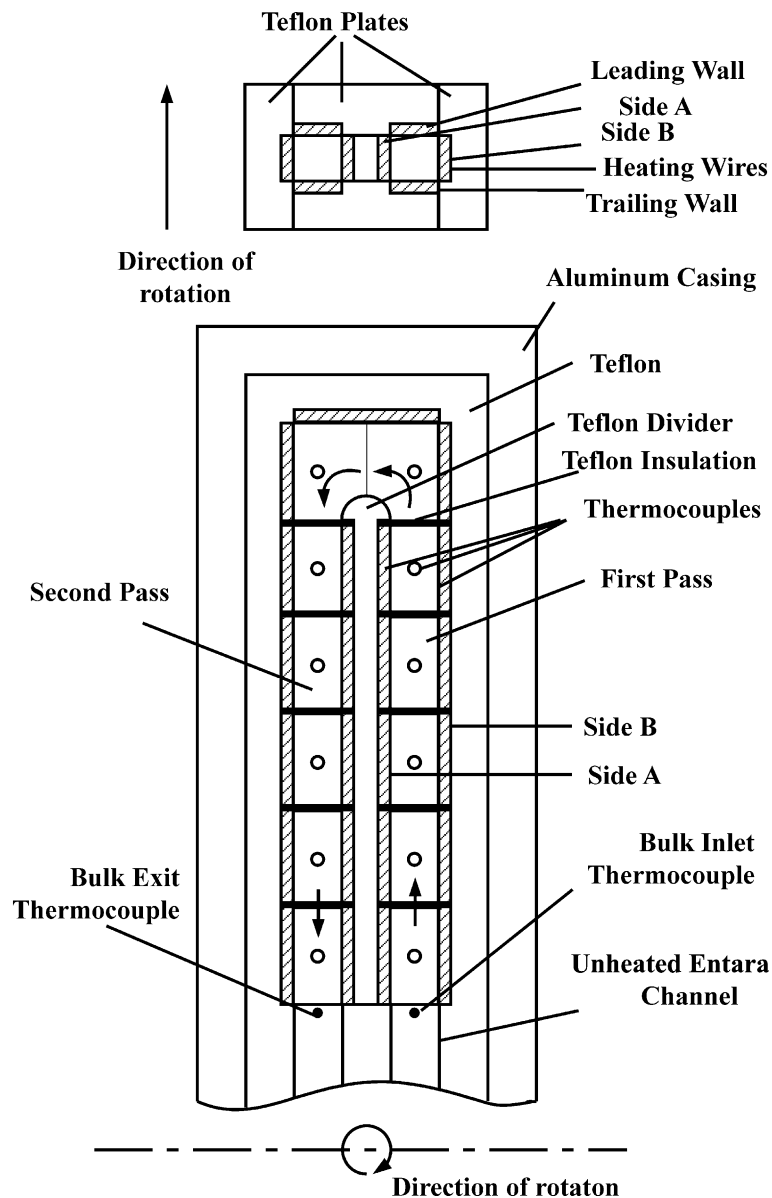
Fig. 2. Cross-sectional view for the channel.

meter, travels through a rotary seal, an aluminum hollow shaft, and a Teflon pipe with a length-to-diameter ratio of 13 to establish a fully developed flow at the entrance of the heat transfer model. The passage surfaces of the heat transfer model consist of electrically heated copper plates. The flow passage of the heat
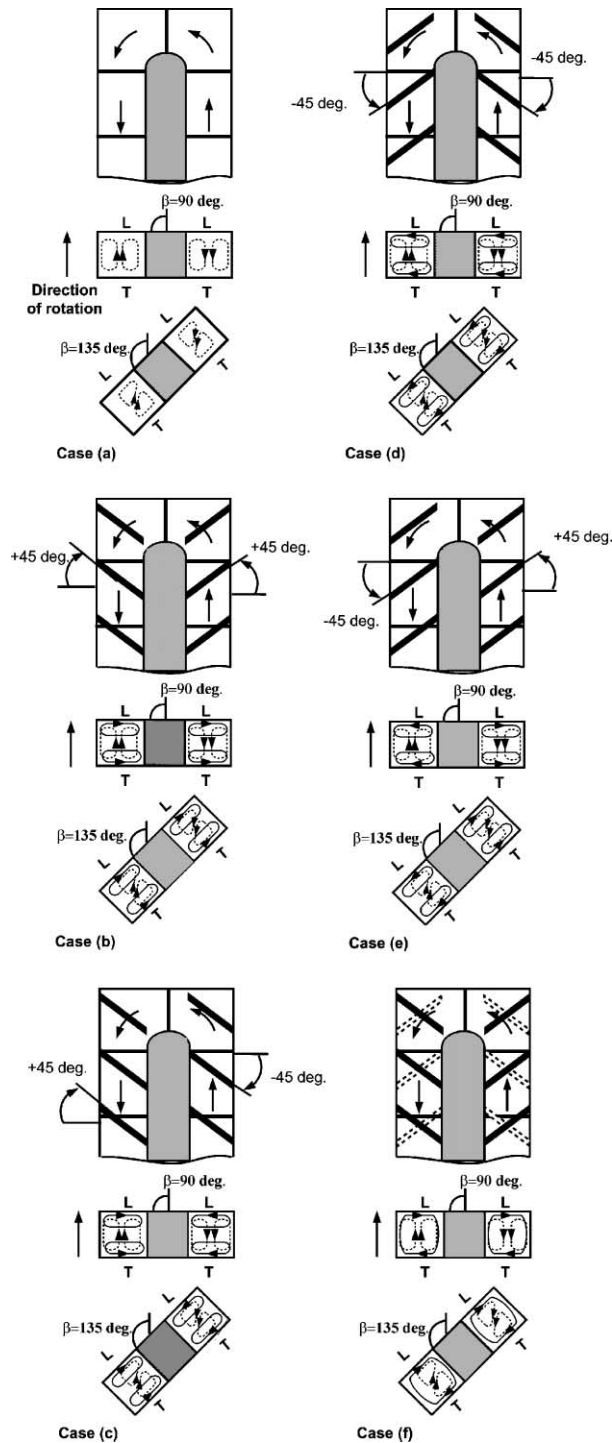
Fig. 3. Conceptual view of the secondary flow vortices induced by rotation, ribs, and channel orientation (dash lines: rotation-induced vortices, solid line: rib-induced vortices).

transfer model is radially outward in the first pass and radially inward in the second pass. Air exhausts into the atmosphere from an opening that is located at the end of the second unheated pass. Slip rings are used to transfer the thermocouple signal to a data logger and power the wire heaters that are laid under the copper plates. A digital photo tachometer measures the rotational speed.

Fig. 2 shows a schematic cross-section view of the two-pass test section without ribs, similar to the test section of Han et al. [14]. The hydraulic diameter of the square test section is 11.7 mm. The heated test section length-to-hydraulic diameter ratio is 24. Each pass is 12 hydraulic diameters long connected by a sharp 180° turn. The flow is radially outward in the first pass and radially inward in the second pass. Each surface has six copper plates, except the two inner surfaces, which have five plates each because of the sharp 180° turn, and the end cap has two plates (48 total). Each copper plate is surrounded around its circumference by a Teflon strip to minimize heat conduction. The copper plates are heated with backside-mounted electric resistive heaters which provide a uniform heat flux. Therefore, a single thermocouple, centrally mounted, can adequately measure the mean temperature of an individual copper plate. One thermocouple is respectively fixed at inlet and exit to monitor the bulk flow temperature.

Fig. 3 shows the rib arrangements, channel orientation ($\beta = 90°$, 135°), and secondary flows being generated by rotation and 45° angled ribs. The conceptual view shows that the secondary flow by rotation is mostly on the bulk flow region, whereas the rib effect is expected to be nearer the rib mounted-surfaces. The brass ribs of the square cross-section are attached to the heated surfaces by high thermal conductive adhesive with negligible contact resistance. The rib height-to-hydraulic diameter ratio (e/D) is 0.125; the rib pitch-to-height ratio (P/e) is 10; and the inlet coolant-to-wall density ratio ($\Delta\rho/\rho$) is around 0.11. Three Reynolds numbers ($Re = 5000$, 10,000, 25,000), based on the hydraulic diameter of the channel, are used. The channel rotates at 550 rpm, resulting in three rotation numbers ($Ro = 0.11$, 0.06, 0.025). The heated surface temperature is around 65 °C, and the inlet air temperature is around 26–29 °C.

3. Data reduction

The local heat transfer coefficient is calculated from the local net heat transfer rate per unit surface area to the cooling air, the local surface temperature on each copper plate, and the local bulk mean air temperature as

$$h = q_{net}/[A(T_w - T_{bx})] \tag{1}$$

Eq. (1) is used for the local leading and trailing surface heat transfer coefficient calculations. The local net heat

transfer rate (q_{net}) is the electrical power generated from the heaters minus the heat loss outside the test section. The electrical power generated from the heater is determined from the measured current and voltage of each section heater. The heat loss is estimated by applying two heat flux rates without airflow in the test section to obtain the characteristic heat loss for each of the isolated rectangular copper plates. The surface area in Eq. (1) is the projected area. The side face areas of the ribs are not included in the projected area. The electrical heaters deliver an approximately uniform heat flux heating condition to the backsides of the copper plates. The local bulk mean temperature that is used in Eq. (1) is found by a linear interpolation between the measured inlet and outlet bulk temperatures. Another way to find the local bulk mean temperature is determined by marching along the test section and calculating the temperature rise from the local net heat input through each set of four heated surfaces. The differences between the calculated and the measured outlet bulk mean temperature are within 1–2 °C in all of the cases.

To reduce the influence of the flow Reynolds number on the heat transfer coefficient, the local Nusselt number of the present study is normalized by the Nusselt number for fully developed turbulent flow in smooth circular tubes with no rotation correlated by Dittus-Boelter/ McAdams as:

$$Nu/Nu_o = (hD/k)/[0.023 \times Re^{0.8} \times Pr^{0.4}] \tag{2}$$

The Prandtl number for air is $Pr = 0.72$. Air properties are based on the mean bulk air temperature.

The uncertainty of the local heat transfer coefficient is affected by the local wall-to-coolant temperature difference and the net heat input into the coolant flow from each heated copper plate. The uncertainty of the local heat transfer coefficient increases for low wall-to-coolant temperature difference ($T_w - T_{bx}$) and for low net heat input. Based on the method described by Kline and McClintock [23], the typical uncertainty in the Nusselt number is estimated to be less than 8% for Reynolds number larger than 10,000. However, the maximum uncertainty could be up to 20% for lower heat transfer coefficients for the lowest Reynolds number tested.

4. Results and discussion

In order to understand the heat transfer distribution inside the two-pass square channel with 180° turn, it is extremely important to discuss the conceptual views of the secondary flow behavior. Fig. 3 shows conceptual views for the secondary flow patterns of smooth and ribbed rotating two-pass square channels. Fig. 3a shows the smooth channel that rotates at $\beta = 90°$ with respect to the direction of rotation. Two symmetric cells of

counter rotating secondary flow (dotted line) are induced by the Coriolis force. In the first pass of the channel, the fluid moves in a radially outward direction, and the effect of the Coriolis force directs the coolant from the core toward the trailing surface. This causes an increase of the heat transfer from the trailing surface and a decrease in the heat transfer from the leading surface. However, in the second pass, the opposite situation can be seen when the fluid moves in a radially inward direction and the Coriolis force directs the coolant toward the leading surface, and causes an increase of heat transfer from the leading surface and a decrease in the heat transfer from trailing surface. When the channel is positioned at the $\beta = 135°$ orientation, the secondary flow vortices are asymmetric and migrate diagonally away from the corner region of the outer-leading surface toward the center in the first passage, and from the corner region of the outer-trailing surface toward the center in the second passage.

Fig. 3b–e show four different arrangements of the parallel ribs on the same smooth channel. The 45° an-gled ribs are attached to leading and trailing surfaces in parallel sequence so that they are directly opposite each other. Fig. 3b shows the ribs attached to the leading and trailing surfaces at +45°. The figure also shows the secondary flow (dotted line) induced by rotational forces and the secondary flow (solid line) induced by the ribs, which form a flow pattern parallel to the ribs at the surface, traveling along the rib to impinge on the outer surface in the first pass and the inner surface in the second pass. However, the rib-induced secondary flow combines with the rotation-induced secondary flow to create constructive and destructive zones on the leading and trailing surfaces and enhance the heat transfer compared to the smooth surface case. As the channel position is changed to $\beta = 135°$, rib-induced secondary flow does not change, but the rotational secondary flows are shared between the trailing and leading surfaces and side surfaces.

Fig. 3c shows the same channel except that the first pass rib orientation is reversed to become −45° to the main stream flow. In consequence of this change, all
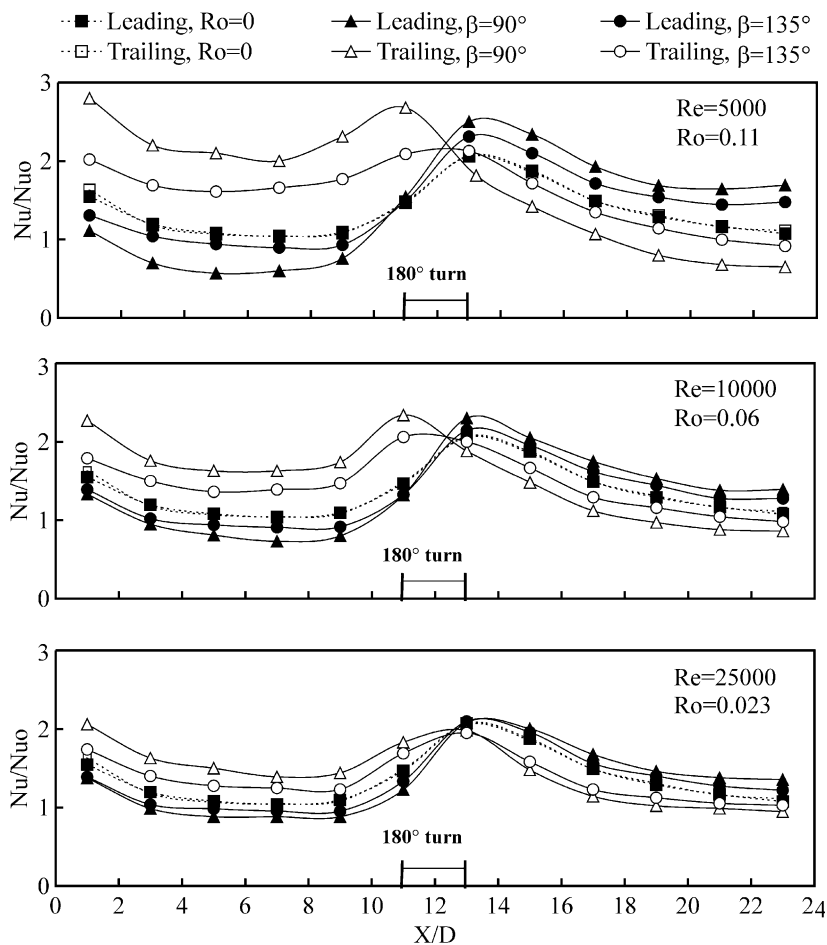
Fig. 4. Regional Nusselt number ratio for case (a).

secondary flows that are induced by rotational forces or ribs are the same as case (b) except the rib-induced secondary flow in the first pass is reversed due to changing in the rib orientation in the first pass. For case (d) as seen in Fig. 3d, the first pass rib orientation is kept as case (c), but second pass rib orientation is reversed to −45°, which implies that the rib-induced secondary flow direction will be reversed in the second pass. Finally, Fig. 3e shows that the first pass rib orientation is reversed to +45° compared to case (d), while the second pass rib orientation is kept the same.

Fig. 3f shows the crossed rib case (the ribs on two opposite surfaces of the cooling channels are in crossed orientation). It is conjectured that the crossed rib case creates a single cell of secondary flow. This rib-induced single cell, secondary flow vortex does not mix well with the core flow (cold fluid) and merely restricts heat transfer because there is less temperature gradient left near the surfaces. In this case with rotation, the rotation-induced, two-cell, secondary flow vortices interact with the single cell secondary flow generated by the crossed ribs. The authors believe this interaction produces low heat transfer performance because the single cell secondary flow vortex minimizes the effect coming from

rotation by suppressing flow impingement on the first pass trailing surface and second pass leading surface, thereby restricting mixing with the core for both trailing and leading surfaces in both passes. Therefore, it is expected that the crossed rib cases will result in less heat transfer enhancement than the parallel rib cases.

Figs. 4–8 show the regionally averaged Nusselt number ratios (Nu/Nu_o) from leading and trailing surfaces for three Reynolds numbers (5000, 10,000, 25,000), rotating and non-rotating, and two channel orientations ($\beta = 90°$, 135°).

4.1. Smooth surface case

Fig. 4 shows the results of Nusselt number ratios from leading and trailing surfaces for the smooth surface case. The non-rotating heat transfer ratio decreases monotonically for both leading and trailing surfaces from 1.6 near the thermal entrance of the first passage to about 1.1 near the downstream $X/D = 9$ and then recovers to 1.6 before the flow enters the sharp 180° turn. The non-rotating heat transfer ratio reaches its highest value of 2.0 right after the sharp 180° turn ($X/D = 13$) due to the secondary flows induced by the 180° turn. The
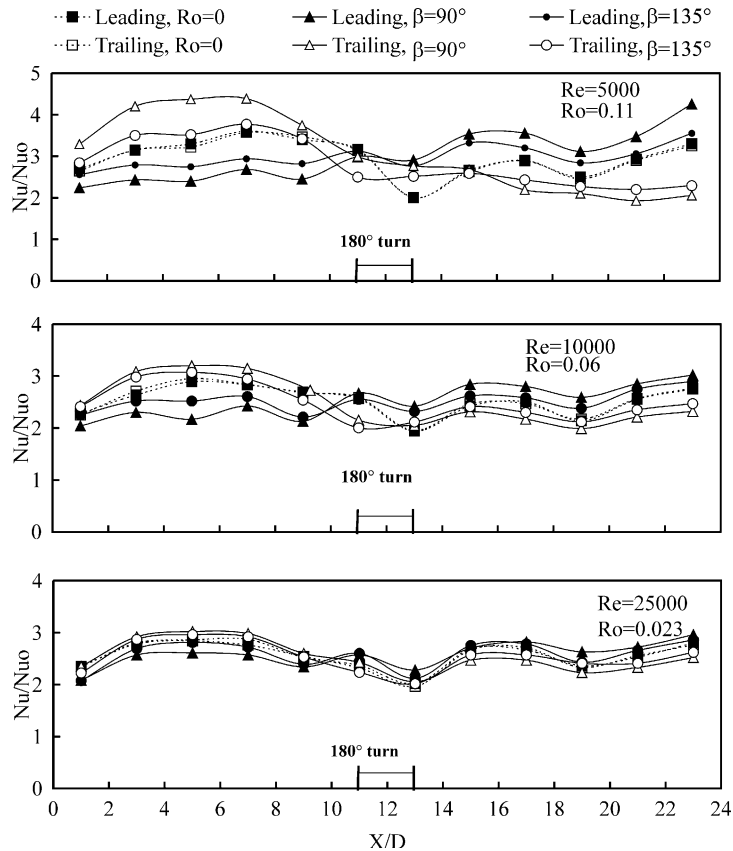
Fig. 5. Regional Nusselt number ratio for case (b).

Nusselt number ratio approaches the fully developed turbulent flow value 1.1 near the second pass outlet region. However, in the rotation case, the Nusselt number ratios from the first pass trailing and second pass leading surfaces are higher than in the non-rotating case, while those from the first pass leading and second pass trailing surfaces are lower. This is because of the rotation-induced secondary flow vortices, as shown in Fig. 3 case (a). At channel orientation $\beta = 90°$, rotation secondary flow vortices produced by Coriolis forces are impinging normally on the first pass trailing surface and the second pass leading surface. However, at channel orientation $\beta = 135°$, the rotation secondary flow vortices are impinging on the first pass trailing-side corner and the second pass leading-side corner, as shown in Fig. 3a. Thus, the Nusselt number ratios for the first pass trailing surface and the second pass leading surface for channel orientation $\beta = 135°$ are lower than the ratios for channel orientation $\beta = 90°$. The opposite situation is observed in the first pass leading surface and the second pass trailing surface: the $\beta = 135°$ case has a higher Nusselt number ratio when compared to the $\beta = 90°$ channel orientation. It is also noticed that the rotation effect on Nusselt number ratios for the second pass is not

as strong as that for the first pass. This is because Coriolis and buoyancy forces move in the same direction in the first pass, while in the second pass they move against each other (see [14]). The results also show that the effect of rotation decreases with increasing Reynolds number (or decreasing rotation number). The above-mentioned results are consistent with the previous study (see [18]).

4.2. 45° parallel rib cases

Fig. 5 shows the Nusselt number ratios for case (b). The results show that the non-rotating Nusselt number ratio is 2.5–3 times that of the non-rotating smooth surface case. This is because of the rib-induced turbulence and secondary flow effects. The Nusselt number ratios for 45° parallel ribs behave completely different from the smooth case. The stationary case results show the peak Nusselt number ratio occurs at the middle of the first pass rather than at the entrance region. The peak Nusselt number ratio occurs in the vicinity of $X/D = 6$ due to the $+45°$ parallel rib, which contains a pair of counter rotating cells, as shown in Fig. 3b. These counter rotating cells travel from the inner surface along the rib and return back to the inner surface, mixing the
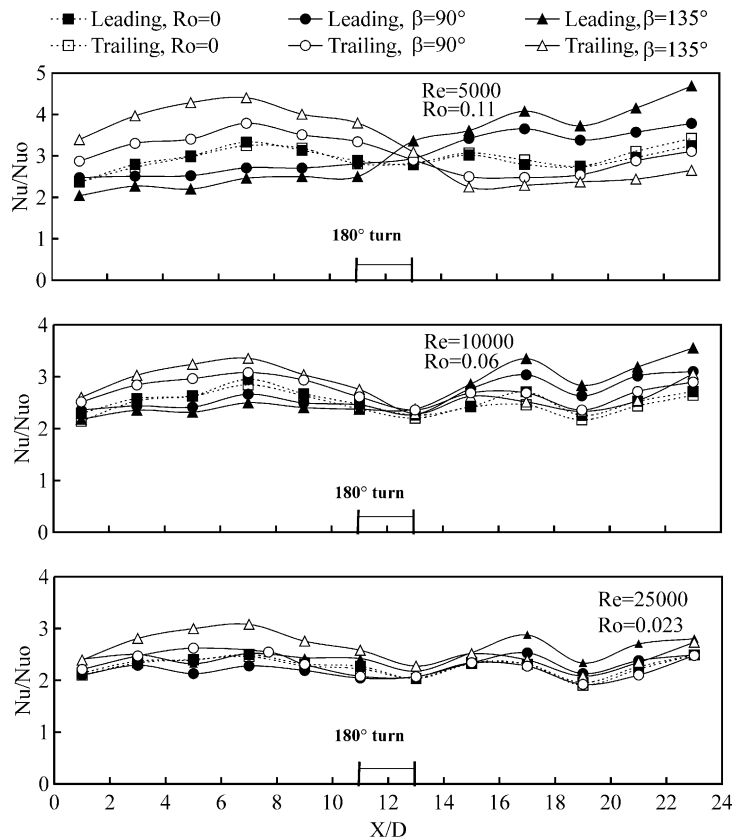
Fig. 6. Regional Nusselt number ratio for case (c).

core cold fluid with the near surface hot fluid to increase the Nusselt number ratios. As the fluid approaches the 180° turn, the Nusselt number ratio decreases as the rib-induced secondary flow effects are influenced by the 180° turn. At the entrance of the 180° turn ($X/D = 11$), the rib trips the boundary layer and enhances the Nusselt number ratio by two times that of the smooth case. As the flow proceeds to the second pass 180° turn ($X/D = 13$), the Nusselt number ratio decreases and almost shows no enhancement compared to the smooth case ($Nu/Nu_o = 2$). It seems that the rib is working as an obstacle against the 180° turning flow. In the second pass, the Nusselt number ratio increases then decreases slightly and increases again toward the exit. The second increase is due to the rib secondary flow dominating in the second pass.

The results also show that rotation significantly increases the Nusselt number ratio on the first pass trailing surface and the second pass leading surface. The rotating Nusselt number ratios from the first pass trailing and second pass leading surface are higher than in the non-rotating case, while those from the first pass leading and second pass trailing surfaces are lower. This is because of the combined effect of the rib-induced secondary flow and the rotation-induced-secondary flow vortices, as shown in Fig. 3 case (b). The Nusselt number ratio has the same trend as the stationary case except the first pass leading surface and the second pass trailing surface are relatively uniform.

For the 135° channel orientation, the results also show that rotation enhances the heat transfer in the first pass trailing surface and second pass leading surfaces,
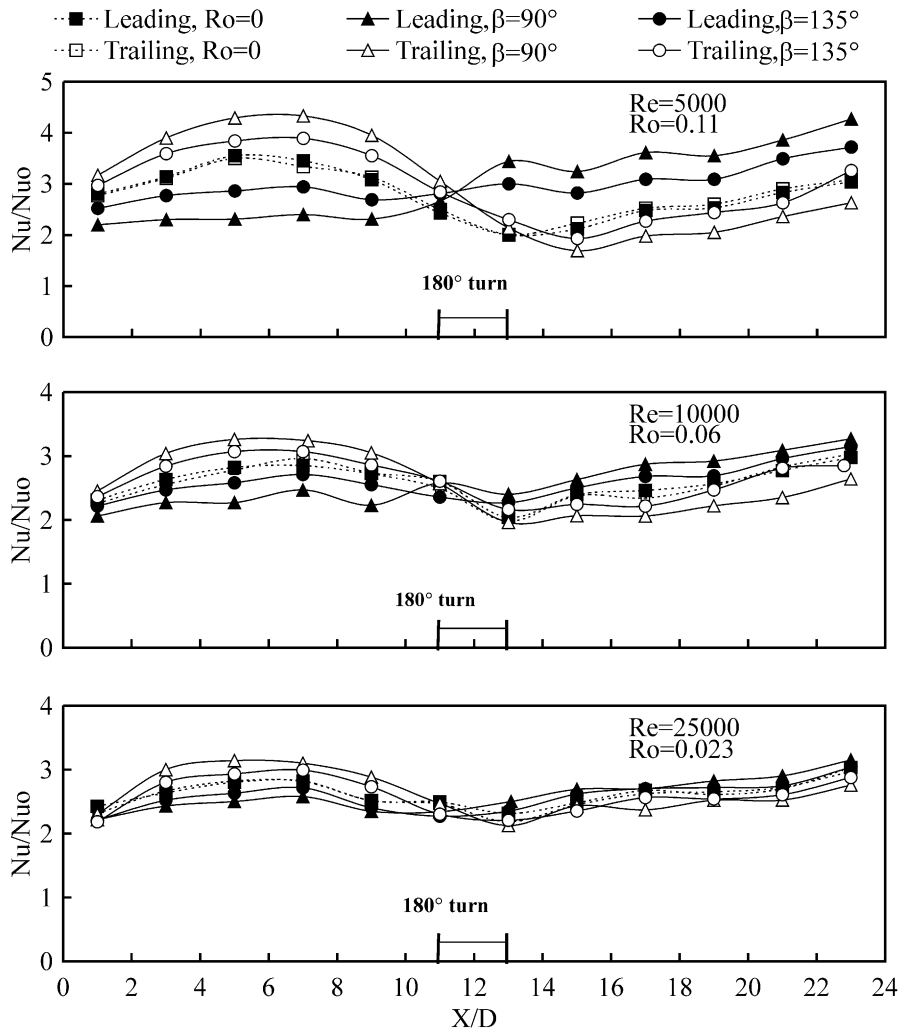
Fig. 7. Regional Nusselt number ratio for case (d).

whereas the heat transfer decreases in the first pass leading and second pass trailing surfaces. In the 135° orientation, the heat transfer surfaces are not orthogonal to the plane of rotation, and the rotational effects are less significant when compared with the 90° orientation, as shown in Fig. 5. The effect of Coriolis forces on the first pass trailing and second pass leading surfaces for the 90° rotation is greater since the two counter vortices are normally incident on the first pass trailing surface and second pass leading surface. Thus, greater differences between leading and trailing Nusselt number ratios in each pass are observed in the 90° orientation. Hence, the difference in Nusselt number ratio between the leading and trailing surfaces are not as significant for the 135° orientation as they are for the 90° orientation. In the 180° turn, the leading surface shows slightly better Nusselt number ratio than the trailing surface. The results also show that the rotation effect decreases with increasing Reynolds number (or decreasing rotation number). The above-mentioned phenomena are consistent with the previous studies (see [17,18]).

Fig. 6 represents case (c). The results show that the first pass Nusselt number ratio behaves as case (b) for rotating and non-rotating cases except at the 180° turn. This can be explained in part by looking to the first pass

in Fig. 3 cases (b) and (c). The conceptual views of the secondary flows show the two counter vortices produced by the Coriolis force effect, and another pair of secondary flow vortices produced by the angled rib that is not transverse to the coolant flow direction. It makes no difference if the rib angle is positive (+45°) or negative (−45°) for regional Nusselt number ratio measurements using full width copper plates. This is because the two secondary flows produced by the Coriolis force and rib-angle effect combine to (i) constructively (same direction) enhance heat transfer for one half of each of the leading and trailing surfaces, and (ii) destructively (opposite direction) reduce heat transfer for the other half of each of the leading and trailing surfaces for either positive or negative angled ribs. The overall performance is the same for the first and second passes in either case. However, as mentioned above, when the fluid approaches the 180° turn, the Nusselt number ratio decreases as the rib-induced secondary flow effect is influenced by the 180° turn. At the entrance of the 180° turn ($X/D = 11$), the case (c) −45° rib orientation guides the fluid rather than trips the boundary layer as in case (b) where the rib orientation is +45°. Therefore, the Nusselt number ratio in case (c) is slightly lower than in case (b). However, in the second pass 180° turn
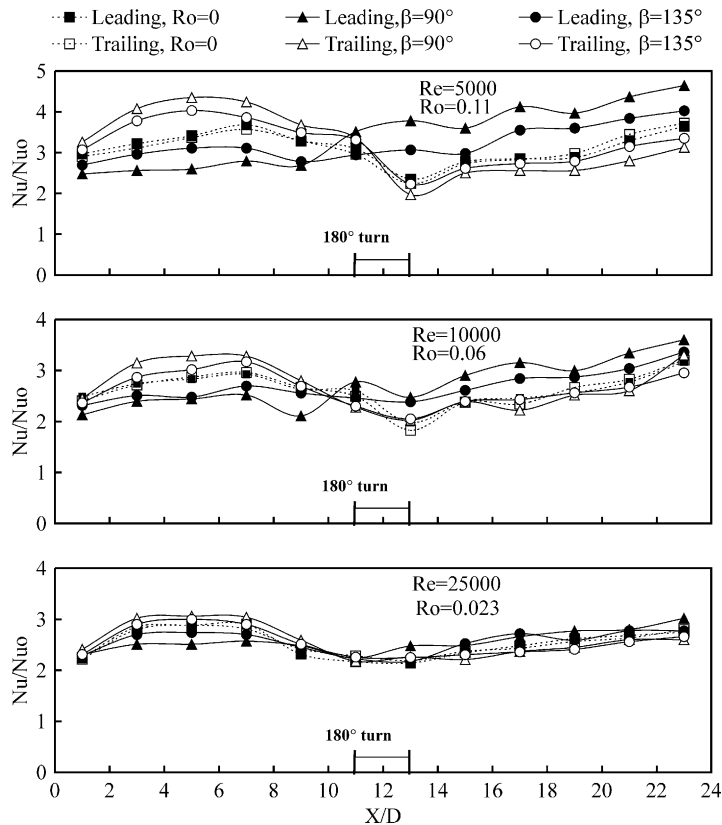
Fig. 8. Regional Nusselt number ratio for case (e).

($X/D = 13$), case (c) exhibits a higher Nusselt number ratio than case (b). This is because case (c) provides a better guide for the 180° turning flow than case (b). In the case (b) first pass ($X/D = 11$), the +45° angled rib trips the boundary layer and increases turbulence at the expense of the fluid momentum. However, in the case (c) first pass ($X/D = 11$), the −45° angled rib guides the fluid rather than tripping the boundary layer and increasing turbulence. As the fluid moves through the second pass, the Nusselt number ratio increases, then decreases and increases again toward the exit. The second increase is due to the rib-induced secondary flow dominating the second pass.

Fig. 7 shows the Nusselt number ratios for case (d). In the first pass, the rib position for cases (c) and (d) are kept the same, while the second pass ribs are reversed (see Fig. 3). The first pass Nusselt number ratios are relatively similar for both cases. In the second pass 180° turn ($X/D = 13$), the Nusselt number ratio shows a lower value compared to case (c), because the −45° rib orientation does not participate as did the +45° rib orientation in case (c) to trip the boundary layer. As the fluid proceeds through the second pass, the Nusselt number ratio continuously increases toward the exit.

Fig. 8 shows the Nusselt numbers for case (e). The Nusselt number ratios in the first pass and second pass show the same trend as case (b) except in the 180° turn. In the first pass 180° turn ($X/D = 11$), the Nusselt number ratio for case (e) is higher than that in case (d); however, the reverse is true in the second pass 180° turn ($X/D = 13$). The reason can be seen from the above-mentioned comparison between case (b) and case (c). In the second pass the Nusselt number ratio increases continuously toward the exit as in case (d).

4.3. 45° crossed rib case

Fig. 9 shows the Nusselt number ratios for the 45° crossed rib case. The results show that the non-rotating Nusselt number ratios on both leading and trailing surfaces are not identical, and the Nusselt number ratios are lower than the parallel rib case. This is similar to those reported by Han et al. [5]. The flow pattern generated by the 45° crossed rib may contain a single cell of secondary flow as shown in Fig. 3 case (f), whereas the 45° parallel rib contains a pair of counter rotating cells. The single cell vortex may not mix well with the core fluid and reduce Nusselt number ratios. The rotation-
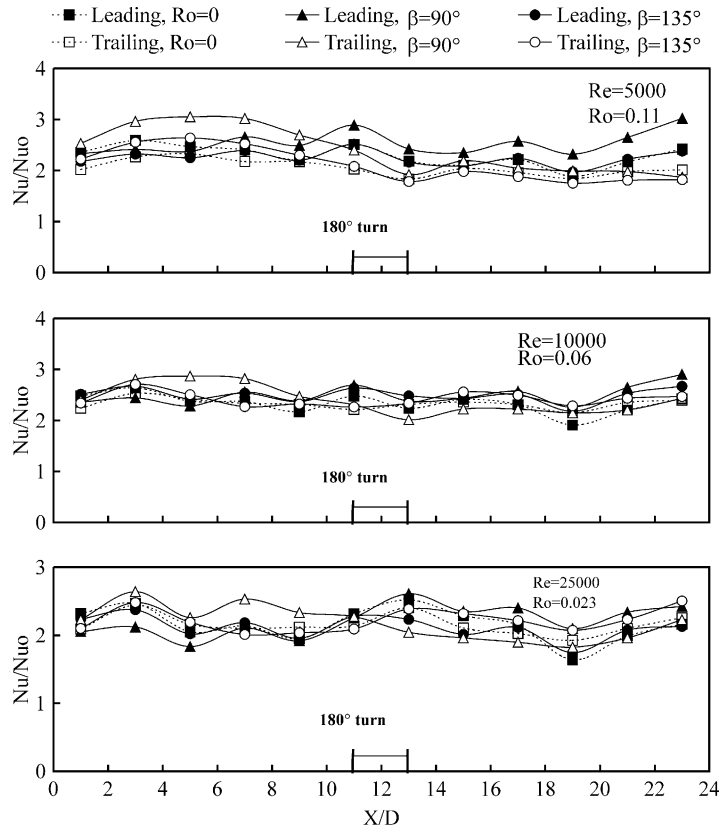
Fig. 9. Regional Nusselt number ratio or case (f).

induced secondary flow vortex pushes the core cold fluid toward the trailing surface in the first pass and the leading surface in the second pass. Thus, it helps to increase the first pass trailing and second pass leading surface heat transfer. However, the effect of rotation is relatively small, and the Nusselt number ratios along the cooling channel are relatively uniform compared with the 45° parallel rib cases.

4.4. Channel averaged Nusselt number ratio

The channel averaged Nusselt number ratios on each pass leading and trailing surfaces are respectively presented for $\beta = 90°$ and 135° in Figs. 10 and 11.

The results in Fig. 10 show that the Nusselt number ratios in the first pass trailing surface increase, while they slightly decrease in the first pass leading surface with an increase in rotation number. However, in the second pass, the Nusselt number ratios on the leading surface increase with rotation number, while on the trailing surface they slightly decrease except for in cases (c) and (e). The results reveal that the parallel and crossed rib cases doubled the averaged Nusselt number

ratios compared to the smooth case. In the first pass leading surface, parallel and crossed rib cases collapse together without showing much variation. Meanwhile, the trailing surface averaged Nusselt number ratios show some variation between parallel and crossed rib cases, especially at higher rotation numbers. Similar behavior can be observed in the second pass leading surface. However, in the second pass trailing surface, case (c) and case (e) show slightly increasing in the Nusselt number ratios, opposite to the other cases. The interaction between the 180° turn, rib orientation, and rotation produces complex flow behavior effecting the Nusselt number ratios. It is clear that under rotation conditions, the Nusselt number ratios are more sensitive to the rib orientation in the first pass trailing and second pass leading surfaces.

Fig. 11 shows the channel averaged Nusselt number ratio on the leading and trailing surfaces for $\beta = 135°$. The results are similar to those for $\beta = 90°$ in trend except that the Nusselt number values on the first pass trailing and the second pass leading surfaces are lower because of the oblique angle of the flow impinging on the surfaces. In general, the parallel rib cases produce
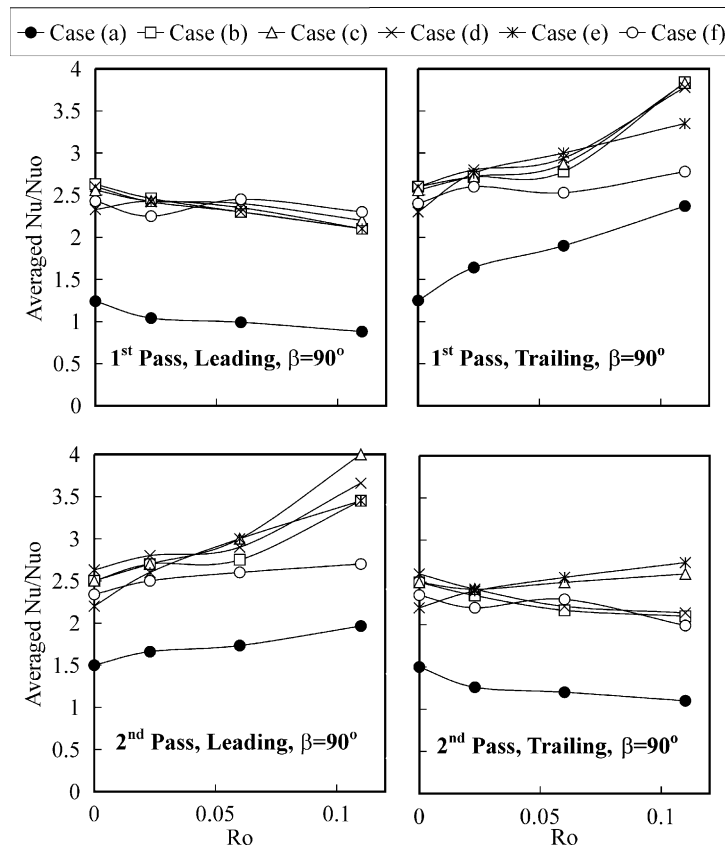
Fig. 10. Averaged Nusselt number ratio on leading and trailing surfaces for $\beta = 90°$.
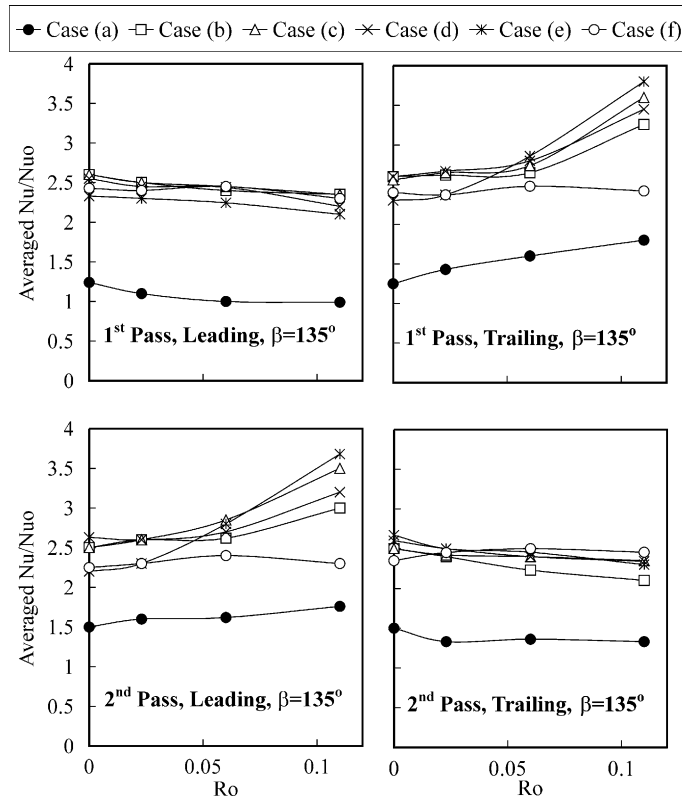
Fig. 11. Averaged Nusselt number ratio on leading and trailing surfaces for $\beta = 135°$.

higher Nusselt number ratios than the crossed rib case, and subsequently higher than the smooth surface case. Rotation-induced secondary flow significantly enhances heat transfer in the first pass trailing and second pass leading surfaces, while it slightly reduces the heat transfer on the first pass leading and second pass trailing surfaces.

4.5. Nusselt number ratio in the 180° turn

Fig. 12 represents Nusselt number ratios for $\beta = 90°$, at two locations ($X/D = 11, 13$) in the 180° turn region. As the flow gets in the 180° turn, centrifugal forces generate secondary flows. These secondary flows can be interrupted by the rib-induced secondary flow before and after the turn. When rotating appears, the Coriolis force adds another complexity. At the end of the first pass (i.e., the corner right before the 180° turn, $X/D = 11$), the Nusselt number ratios for both leading and trailing surfaces show continuous increase with rotation number due to the constructive interaction between the Coriolis force and the 180° turning flow. The slight variation between the Nusselt number ratios of the ribbed cases is due to the rib orientation which is sometimes a trip or a guide for the flow as shown in Fig.

3. At the beginning of the second pass (i.e., the corner right after the 180° turn, $X/D = 13$), the Nusselt number ratios show an increasing trend for the leading surface and a slight increasing trend for the trailing surface. This is because the Coriolis force pushes the fluid towards the leading surface. The variation between the various rib cases is visible with high rotation number, which produces complex interaction among the Coriolis force, rib-induced secondary flow, and 180° turning flow as sketched in Fig. 3. Fig. 13 shows Nusselt number ratios for $\beta = 135°$. The Nusselt number ratios have similar behavior except the effect of the Coriolis force is shared by the other two surfaces (inner and outer). Therefore, the rotational effect on the leading and trailing surfaces' Nusselt number ratios in the 180° turn region are slightly reduced as compared to those for $\beta = 90°$.

5. Conclusions

The influences of five different 45° angled ribs arrangements and channel orientation on the leading and trailing Nusselt number ratio in a two-pass square channel have been reported for rotation numbers rang-
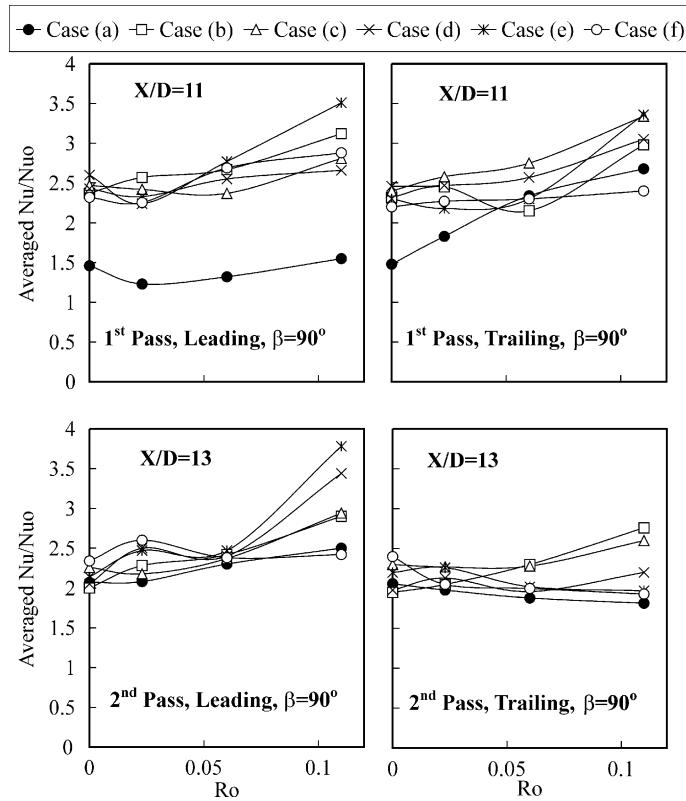
Fig. 12. Effect of rotation number on Nusselt number ratio in 180° turn for $\beta = 90°$.

ing from 0.0 to 0.11 and Reynolds numbers ranging from 5000 to 25,000. The findings are:

1. The local heat transfer coefficient distribution in a rotating frame is different from that of a stationary frame. In general, the Nusselt number ratios in the first pass trailing and second pass leading surfaces increase with an increase in rotation number. The reverse is true for the first pass leading and second pass trailing surfaces. The results of this study confirm the results of previous studies.

2. The Nusselt number ratio differences between the leading and trailing surfaces due to rotation are reduced as the channel orientation changes from $\beta = 90°$ to $\beta = 135°$. Therefore, the Nusselt number ratios for the first pass trailing and second pass leading surfaces for $\beta = 135°$ are lower than the corresponding Nusselt number ratios for the $\beta = 90°$ orientation. However, the Nusselt number ratios for the first pass leading and second pass trailing surfaces for $\beta = 135°$ are slightly enhanced compared to the corresponding Nusselt number ratios for the $\beta = 90°$ channel orientation.

3. The 45° parallel rib arrangements provide higher heat transfer enhancement compared to the 45° crossed rib arrangement for the non-rotating cases. For the rotating cases, the Nusselt number ratios in the first pass trailing and second pass leading surfaces of the 45° parallel ribs are significantly higher than those of the 45° crossed ribs.

4. In four different 45° parallel rib arrangements, cases (c) and (e) tend to provide higher overall Nusselt number ratios than cases (b) and (d), particularly for the increased rotation numbers. The Nusselt number ratio differences among four parallel rib cases are more noticeable in the first pass trailing and second pass leading surfaces than in the first pass leading and second pass trailing surfaces.

5. In general, the Nusselt number ratios in the 180° turn region increase with an increase in rotation number. The Nusselt number ratio differences in the 180° turn region among different angled rib orientations also increase with the increase in rotation number.

It should be noted that the present results are based on the rotating channel with a long length entrance and lower rotation numbers. However, typical coolant channels in modern gas turbine blades have a sharp entrance and higher rotation numbers.
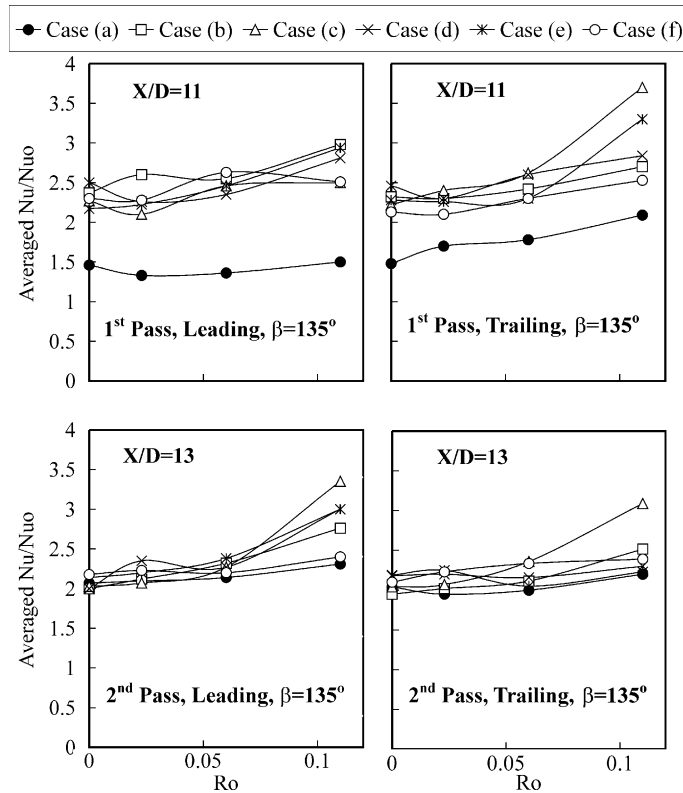
Fig. 13. Effect of rotation number on Nusselt number ratio in 180° for $\beta = 135°$.

References

[1] D.E. Metzger, M.K. Sahm, Heat transfer around sharp 180° turns in smooth rectangular channels, ASME J. Heat Transfer 108 (1986) 500–506.

[2] C.S. Fan, D.E. Metzger, Effects of channel aspect ratio on heat transfer in rectangular passage sharp 180° turn, ASME Paper No. 87-GT-113, 1987.

[3] J.C. Han, P.R. Chandra, S.C. Lau, Local heat/mass transfer in distributions around sharp 180 deg. turns in two-pass smooth and rib-roughened channels, ASME J. Heat Transfer 110 (1988) 91–98.

[4] J.C. Han, P. Zhang, Effect of rib-angle direction on local mass transfer distribution in a three-pass rib-roughened channel, ASME J. Turbomach. 113 (1991) 123–130.

[5] J.C. Han, Y.M. Zhang, C.P. Lee, Augmented heat transfer in square channels with parallel, crossed, and V-shaped angled ribs, ASME J. Heat Transfer 113 (1991) 590–596.

[6] S.V. Ekkad, J.C. Han, Detailed heat transfer distribution in two-pass square channels with rib turbulators, Int. J. Heat Mass Transfer 40 (11) (1997) 2525–2537.

[7] S.V. Ekkad, Y. Huang, J.C. Han, Detailed heat transfer distribution in two-pass square channels with rib turbulators and bleed holes, Int. J. Heat Mass Transfer 41 (11) (1998) 3781–3791.

[8] J.H. Wagner, B.V. Johnson, T.J. Hajek, Heat transfer in rotating passage with smooth walls and radial outward flow, J. Turbomach. 113 (1991a) 42–51.

[9] J.H. Wagner, B.V. Johnson, F.C. Kooper, Heat transfer in rotating passage with smooth walls, J. Turbomach. 113 (3) (1991b) 321–330.

[10] M.E. Taslim, A. Rahman, S.D. Spring, An experimental investigation of heat transfer coefficients in a spanwise rotating channel with two opposite rib-roughened walls, ASME J. Turbomach. 113 (1991) 75–82.

[11] M.E. Taslim, L.A. Bondi, D.M. Kercher, An experimental investigation of heat transfer in an orthogonally rotating channel roughened with 45 deg criss-cross ribs on two opposite walls, ASME J. Turbomach. 113 (1991) 346–353.

[12] B.V. Johnson, J.H. Wagner, G.D. Steuber, F.C. Yeh, Heat transfer in rotating serpentine passage with trips skewed to the flow, ASME J. Turbomach. 116 (1994a) 113–123.

[13] B.V. Johnson, J.C. Wagner, G.D. Steuber, F.C. Yeh, Heat transfer in rotating serpentine passage with selected model orientations for smooth or skewed trip walls, ASME J. Turbomach. 116 (1994b) 738–744.

[14] J.C. Han, Y.M. Zhang, K. Kalkuehler, Uneven wall temperature effect on local heat transfer in a rotating two-pass square channel with smooth walls, ASME J. Heat Transfer 115 (4) (1993) 912–920.

[15] Y.M. Zhang, J.C. Han, J.A. Parsons, C.P. Lee, Surface heating effect on local heat transfer in a rotating two-pass square channel with 60° angled rib turbulators, ASME J. Turbomach. 117 (1995) 272–280.

[16] J.A. Parsons, J.C. Han, Y.M. Zhang, Wall heating effect on local heat transfer in a rotating two-pass square channel with 90° rib turbulators, Int. J. Heat Mass Transfer 37 (9) (1994) 1411–1420.

[17] J.A. Parsons, J.C. Han, Y.M. Zhang, Effects of model orientation and wall heating condition on local heat transfer in a rotating two-pass square channel with rib turbulators, Int. J. Heat Mass Transfer 38 (7) (1995) 1151–1159.

[18] S. Dutta, J.C. Han, Local heat transfer in rotating smooth and ribbed two-pass square channels with three channel orientations, ASME J. Heat Transfer 118 (1996) 578–584.

[19] S. Dutta, J.C. Han, C.P. Lee, Local heat transfer in a rotating two-pass ribbed triangular duct with two model orientations, Int. J. Heat Mass Transfer 39 (1996) 707–715.

[20] C.W. Park, S.C. Lau, Effect of channel orientation of local heat (mass) distributions in a rotating two-pass square channel with smooth walls, ASME J. Heat Transfer 120 (1998) 624–632.

[21] C.W. Park, C. Yoon, S.C. Lau, Heat (mass) transfer in a diagonally oriented rotating two-pass channel with rib-roughened walls, ASME J. Heat Transfer 122 (2000) 208–211.

[22] J.C. Han, S. Dutta, S.V. Ekkad, Gas Turbine Heat Transfer and Cooling Technology, Taylor and Francis, New York, 2000.

[23] S.J. Kline, F.A. McClintock, Describing uncertainty in single-sample experiments, Mech. Eng. 75 (1953) 3–8.